Molecular Electron Transport Changes upon Structural Phase Transitions in Alkanethiol Molecular Junctions

Kyoungja Seo and Hyoyoung Lee*

National Creative Research Initiative, Center for Smart Molecular Memory, Electronics and Telecommunications Research Institute (ETRI), 161 Gajeong-dong, Yuseong-gu, Daejeon 305-350, Korea

ABSTRACT We demonstrated structural phase dependency of conductance across thiolate self-assembled monolayers (SAMs) in different junctions. A structural phase transition from a hexagonal closed phase to a striped phase in 1-octanethiol (OT) and 1,8-octanedithiol (ODT) SAMs was revealed by high resolution scanning tunneling microscopy (STM) images. Electron tunneling characteristics were measured through STM-based individual molecular junctions and micropore-based large molecular junctions. The tunneling barrier height and the tunneling decay constant of the molecular junctions were used as measures of the intermolecular coupling for different structural phases of the thiolate SAMs. Electron transport through ODT SAMs was found to be more sensitive than that through OT SAMs, according to the structural phase transition. These results suggest that (1) the structural phase transition in the SAM induces a change in the electron tunneling distance through the pathway of through-bond tunneling and through-space tunneling, leading to a change in the tunneling barrier of molecular junctions, and (2) integrated intermolecular coupling in a large molecular junction leads to a significant change of the electron transport between two structural phases.

KEYWORDS: molecular electronics · self-assembled monolayer · structural phase transition · molecular junction · electron transport

The electrical and chemical nature of organic thiol molecules in self-assembled monolayers (SAMs) on metal have been studied in relation to applications of molecular electronics.[1,2] To shed light on the transport mechanisms through molecules, current−voltage ($I-V$) characteristics in molecular junctions (metal−molecule−metal) have been studied extensively.[1,3−8] In particular, alkanethiol and alkanedithiol were used as simple model systems to verify effects such as molecular length, metal work function, applied bias, and contact property on electron transport in molecular junctions based on SAMs.[3,9−11] Alkanethiol (or alkanedithiol) generally forms a highly packed SAM on gold at room temperature. The sulfur−gold binding and the intermolecular interaction determine the structural phase of the thiolate SAMs (*i.e.*, alkanethiol and alkanedithiol). These two factors influence electron transport across the thiolate SAM *via* electronic coupling of molecular orbitals and gold (through-bond tunneling) and *via* intermolecular coupling between neighboring molecules (through-space tunneling).[12] Strong electronic coupling of sulfur atoms to gold atoms in alkanethiol SAMs enhances electron transport *via* through-bond tunneling.[12,13] Furthermore, molecular tilt in these SAMs enhances the contribution of through-space tunneling by intermolecular coupling, and the molecular conductance across the SAMs decreases relatively.[14] Atomic force microscopy (AFM) was used to explain relative through-space tunneling in thiolate SAMs with different alkyl chains.[5] Inconsistent with a small molecular junction (*e.g.*, scanning probe microscopy (SPM)-based junctions), however, conductance across SAM-based molecular junctions (or molecular nanodevices) having a large area junction is strongly influenced by the local molecular environment induced by neighboring molecules.[10] Nonetheless, the influence of neighboring molecules such as intermolecular coupling on molecular conductance in thiolate SAMs has not been clearly determined in either type of molecular junctions (*e.g.*, the influence of junction area size).

Thiolate SAMs have different structural phases under given conditions (*e.g.*, heat treatment during or after self-assembly).[15−17] For example, thermal diffusion of the surface gold atoms results in a decrease of the number of gold vacancy islands (or pits) under a vacuum and a structural phase transition from high-density phases to low-density striped phases.[17,18] The molecular orientation of the SAMs is changed with structural phase transition, and molecular electron transport characteristics are varied by different intermolecular coupling induced in each structural phase. Furthermore, intermolecular coupling

*Address correspondence to hyoyoung@skku.edu.

Received for review December 23, 2008 and accepted July 30, 2009.

Published online August 11, 2009.
10.1021/nn8008917 CCC: $40.75

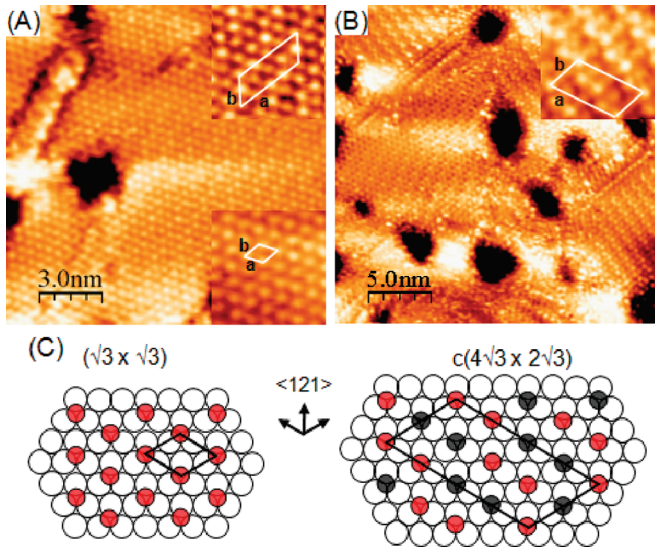

Figure 1. (A, B) STM images of 1-octanethiol (OT) and 1,8-octanedithiol (ODT) SAMs on Au(111), respectively. Image sizes: (A) 15.2 × 15.2 nm² (inset: 3.3 × 3.3 nm²) and (B) 25 × 25 nm² (inset: 3.2 × 3.2 nm²). (C) Representative unit cells of (√3 × √3) and c(4√3 × 2√3) lattices. Open circles represent the surface Au atoms and solid circles represent the sulfur head groups. The SAMs were prepared in a 1 mM solution at room temperature for 2 h. The images were obtained at a constant tunneling current of 20 pA with a tip bias of 1.0 V in a vacuum. The set of arrows indicates the ⟨121⟩ direction of Au(111).

effects arising in different structural phases on electronic transport will be significant in a large molecular junction. However, variation in tunneling characteristics such as electron tunneling barrier of various molecular junctions according to different structural phases has not been addressed, despite that a comprehensive understanding of structural transition-induced molecular electron transport is a very important issue in molecular electronics.

The aim of the present study is to elucidate the relation between structural phase transition and electron transport of molecules on monolayers. We demonstrate structural phase dependency of conductance across thiolate SAMs in given molecular junctions (*i.e.*, individual and large molecular junctions). The molecular electron tunneling characteristics for each structural phase are compared with *I*−*V* curves obtained *via* scanning tunneling microscopy (STM)-based analyses of individual molecular junctions and a micropore-based large molecular junction. The tunneling characteristics (*e.g.*, the tunneling barrier height and the tunneling decay constant) are verified as a measure of the intermolecular coupling for different structural phases of the thiolate SAMs. The differences or similarities observed *via* the STM- and micropore-based junctions for phase-dependent electronic characteristics will provide insight into the effects of intermolecular coupling on tunneling characteristics according to a change of monolayer phases for monolayer-based molecular electronic applications.

RESULTS AND DISCUSSION

Structural Phase Transition. 1-Octanethiol (OT) and 1,8-octanedithiol (ODT) SAMs on Au(111) were prepared at room temperature, and well-ordered structure phases were characterized by high-resolution STM images, as shown in Figure 1A,B. From molecularly resolved images (the insets of Figure 1), the measured lattice constants for the phase structure are determined to be $a = 4.9$ Å and $b = 4.9$ Å, and the angle between lattice vectors is 60°. This results in a ($\sqrt{3} \times \sqrt{3}$) structure, ($a = \sqrt{3}a$Au(111), $b = \sqrt{3}a$Au(111), where aAu(111) = 2.89 Å), and a super lattice c($4\sqrt{3} \times 2\sqrt{3}$) structure, ($a = 4\sqrt{3}a$Au(111), $b = 2\sqrt{3}a$Au(111)), consistent with well-known ordered phases of *n*-alkanethiol in SAMs on Au(111).[19,20] These STM images reveal that ODT molecules assemble in an upright-phase rather than looped- or flat-phases in the SAMs. The ODT SAMs have the same ordered structures as OT SAMs on Au(111), but the monolayer consists of relatively small molecular domains. Representative unit cells for ($\sqrt{3} \times \sqrt{3}$) and c($4\sqrt{3} \times 2\sqrt{3}$) structures (hexagonal closed phases) are depicted in Figure 1C, from which a local surface coverage of 0.33 ML (monolayer) is defined with respect to the atomic density of Au(111), corresponding to a local surface concentration of 4.6×10^{14} molecules cm^{-2}.

To implement the structural phase transition on OT and ODT SAMs, 1 mM hot OT and ODT solutions were used. In the solutions, the molecules were constantly supplied to the surface to reach optimum conditions at a given temperature, even though desorption of chemisorbed molecules takes place. Following 2 h-annealing in the solutions at 333 K, the ordered ($\sqrt{3} \times \sqrt{3}$) and c($4\sqrt{3} \times 2\sqrt{3}$) structures still dominate the OT SAMs, but disordered and striped domains appear at the boundaries of the ordered domains and the gold vacancy islands (Figure S1, Supporting Information). However, after 2 h-annealing in the solutions at 343 K, the structural phase transition is completed, and only a striped phase is found (Figure 2A,B). This structural phase transition from a high-density hexagonal closed phase to a low-density striped phase is consistent with thermal annealing results obtained for alkanethiol SAMs on Au(111) under a vacuum.[18] In OT SAMs, three rotational domains of the striped phase are oriented at 120° to each other, reflecting the 3-fold symmetry of Au(111). From the insets of Figure 2, the measured lattice constants for the phase structure are determined to be $a = 18$ Å and $b = 4.9$ Å and the angle between lattice vectors is 90 ± 1°. This results in a ($6 \times \sqrt{3}$) structure, ($a = 6a$Au(111), $b = \sqrt{3}a$Au(111)). A representative unit cell for the ($6 \times \sqrt{3}$) structure is depicted in Figure 2C. The molecular row distance of A−C (9.0 Å) is consistent with the measured distance in the inset image of Figure 2A. Furthermore, as revealed by a cross-sectional analysis (Figure 2D) of the inset image of Figure 2B, adsorption sites of the ODT molecules (Figure

2E) are different from those of the OT molecules (Figure 2C). The molecular row distance of A′−C′ (10.5 Å) is nearly the same as the measured distance (10.3 Å) in the proposed model in Figure 2E. The (6 × √3) structures have one missing molecular row every four rows as compared to the (√3 × √3) and c(4√3 × 2√3) structures. From the proposed unit cells, a local surface coverage of 0.25 ML for the (6 × √3) structures is defined with respect to the atomic density of Au(111), corresponding to a local surface concentration of 3.5 × 10^{14} molecules cm^{-2}.

STM images and cross-sectional analyses of the images for the striped phases reveal that OT and ODT molecules do not lay flat on the surface. Given that the measured lattice constant (*e.g.*, a = 18 Å) is not consistent with the molecular lengths of OT (11 Å) and ODT (12.5 Å), it can be concluded that the OT and ODT molecules in the striped phases will be oriented upright with a tilt to the surface normal. The molecular orientation angle is expected to be larger in the striped phases than in the hexagonal closed phases. Striped molecular rows in the ODT SAM are kinked over a short distance (Figure S2, Supporting Information). These structural differences (*e.g.*, orientation of molecules) will influence electron tunneling in molecular junctions.

In addition, the structural phase transition-induced molecular orientation on OT and ODT SAMs was detected by water contact-angle measurements (Table S1, Supporting Information). Before thermal annealing, the water contact angle on the OT SAM was relatively larger than that of the ODT SAM due to the hydrophobic outer methyl groups of OT and the hydrophilic outer thiol groups of ODT. After thermal annealing, however, the water contact angle on the OT SAM became smaller due to an increase of the surface hydrophilicity. This indicates outward exposure of methylenes ($(CH_2)_n$) of the alkyl backbone, induced by the structural phase transition from the hexagonal closed to striped phases. Contrary to the case of the OT SAM, the exposure of the methylenes will allow a decrease of the surface hydrophilicity of the ODT SAM. Thus, the surface chemical nature (hydrophobicity or hydrophilicity) confirms that the OT and ODT molecules will be oriented with a larger tilt angle in the striped phase than in the hexagonal closed phase.

Phase-Dependent *I*−*V* Characteristics. STM- and SAM-based molecular junctions have been extensively used for electronic characterization of molecules.[21] The molecular junctions on thiolate SAMs (*e.g.*, STM tip/alkylthiolate/gold substrate and gold top electrode/single alkylthiolate molecule SAM/gold bottom electrode) are considered to be a metal−insulator−metal (M−I−M) junction.[6] The Simmons model is the simplest M−I−M tunneling model and can be applied to describe the electron transport through a molecular junction with molecules having HOMO (the highest occupied molecular orbital) and LUMO (the lowest unoccupied molecular orbital) energy levels.[6,9,22] According to the Simmons model, tunneling currents through the molecular barrier in the direct tunneling regime are described by the following equation:[7,23]

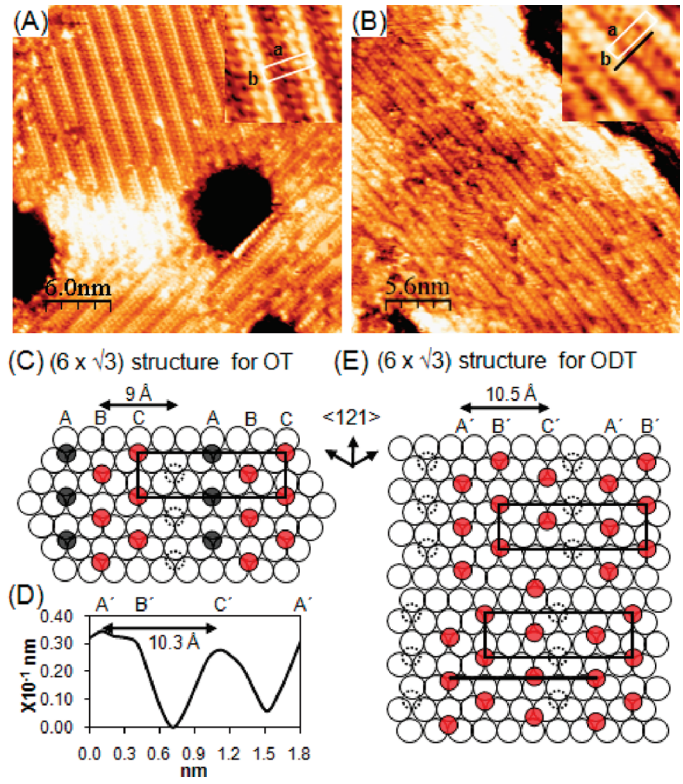

Figure 2. (A) (50.2 × 50.2 nm²) STM image of a OT SAM on Au(111) (inset: 4.4 × 4.4 nm²). (B) (28.0 × 28.0 nm²) STM image of a ODT SAM on Au(111) (inset: 4.0 × 4.0 nm²). The SAMs were prepared in a 1 mM solution at room temperature for 2 h and subsequently immersed at 343 K for 2 h. The images were obtained at a constant tunneling current of 20 pA with a tip bias of 1.0 V under a vacuum. (C) A proposed unit cell with a (6 × √3) lattice respective to panel A. Open circles represent the surface Au atoms and solid circles represent the sulfur head groups. Dotted circles indicate missing molecules. (D) A line profile of the STM image (B) marked as a black line in the inset of panel B. (E) A proposed unit cell with a (6 × √3) lattice respective to panel B. A set of arrows indicates the ⟨121⟩ direction of Au(111).

$$I \approx \frac{e}{4\pi^2\hbar d^2}\left\{\begin{matrix}\left(\Phi_B - \frac{eV}{2}\right)A \\ -\left(\Phi_B + \frac{eV}{2}\right)C\end{matrix}\right\}$$

where

$$A = \exp\left[-\frac{2\sqrt{2m}}{\hbar}\alpha\sqrt{\left(\Phi_B - \frac{eV}{2}\right)}d\right]$$

$$C = \exp\left[-\frac{2\sqrt{2m}}{\hbar}\alpha\sqrt{\left(\Phi_B + \frac{eV}{2}\right)}d\right]$$

and m is the electron mass, d is the barrier width, Φ_B is the barrier height, V is the applied bias, $\hbar$ is Planck's constant, and α is an adjustable parameter. The tunneling decay constant β at zero voltage is determined *via* the following equation:[7]

$$\beta = \frac{2\sqrt{2m}}{\hbar}\alpha\sqrt{\Phi_B} \approx 1.03\alpha\sqrt{\Phi_B}$$

The electron tunneling rate through the molecular junction decreases exponentially with an increase of the molecular length, and the model predicts a decrease in the conductance with an increase of Φ_B and β. Simmons fitting for estimation of the electronic transport properties of the barrier height and the tunneling decay constant has been reliably used in comparisons of models with experimental analyses.[6,7,9] Thus, in this work nonlinear least-squares fitting to fit the equation from the Simmons model to an experimental $I-V$ curve was performed for different structural phases of each thiolate SAM.

The contacts in molecular junctions strongly influence the measured $I-V$ characteristics.[2] Thus, a control experiment was performed (Figure S3, Supporting Information), which revealed that the contacts in the STM junctions were precisely controlled. In this work, $I-V$ curves were obtained numerous times on the same individual molecule after taking a molecularly resolved image at a tunneling current as low as 20 pA. The STM tip was positioned on top of the molecules and the $I-V$ characteristics were measured without tunneling current feedback.[24] The current feedback was then restored, and tip-scanning continued after the current−voltage measurement was completed. The measured $I-V$ curves were reproducible.

After successive high-resolution STM imaging of the OT and ODT molecules in different structural phases (Figures 1 and 2) at a tunneling set-point of 20 pA, the $I-V$ curves in the same molecular junctions were measured and averaged for the Simmons fits (Figure 3). The current plots show that tunneling currents through an STM-based junction in the hexagonal closed phase, c(4$\sqrt{3}$ × 2$\sqrt{3}$) (Figure 3A,B), are slightly larger than those of the striped (6 × $\sqrt{3}$) phase (Figure 3C,D) (also see the measured and calculated $I-V$ curves on a log scale, Figure S4 in Supporting Information). The molecular lengths used in the fitting are 13.3 and 14.8 Å for OT and ODT, respectively, including Au-thiol bond length.[7,25] Adjusting two parameters, Φ_B and α,[7] the Simmons model was fitted to the measured $I-V$ curves in different structural phases of OT and ODT SAMs (Figure 3A−D). Curves fitted to the measured $I-V$ curves were obtained using $\alpha = 1$, a simple rectangular model,

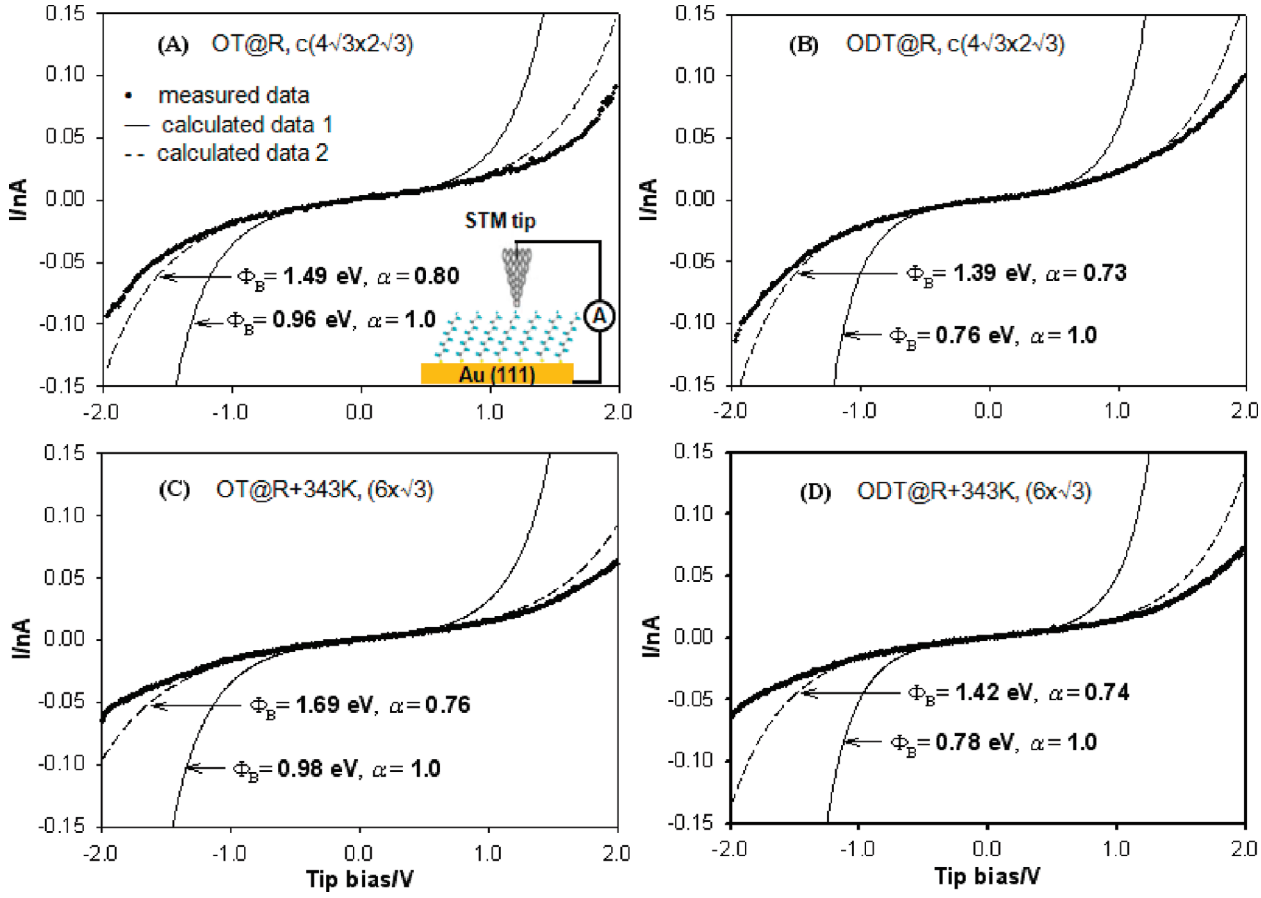

Figure 3. Measured $I-V$ characteristics (a black dotted line) obtained through individual molecular junctions with respect to the structural phases of OT and ODT SAMs on Au(111) and the calculated $I-V$ curves as solid ($\alpha = 1$) and dashed lines ($\alpha \neq 1$) with the Simmons fitting. The SAMs were prepared (A, B) at room temperature (respective to a c(4$\sqrt{3}$ × 2$\sqrt{3}$) phase) and additionally immersed (C, D) at 343 K (respective to a (6 × $\sqrt{3}$) phase) in a 1 mM solution. Current is plotted against a tip-bias voltage on a linear scale. Measured $I-V$ curves are the average of 25 independent curves for each SAM. A modified rectangular model ($\alpha \neq 1$) is fitted well to the experimental data (at a bias region of ±1.0 V). The inset in panel A is illustration of an STM-based molecular junction.

and $\alpha \neq 1$, a modified rectangular model.[7,9] The molecular electronic characteristics through each monolayer phase were compared with the tunneling barrier height (Φ_B) and the estimated tunneling decay value (β) from the Simmons fit curves (Table S2A, Supporting Information). The $I-V$ curves were averaged with 25 independent curves measured in each molecular junction at a bias region of ± 2.0 V. In the application of $\alpha = 1$, a simple rectangular model, the Simmons fit curves for the thiol molecular junctions were fitted at only a limited region of $-0.5 < V < +0.5$. Thus, the curves fitted with $\alpha = 1$ were not fitted well to the experimental data as compared with the curves fitted with $\alpha \neq 1$ (Figure 3). In the case of $\alpha \neq 1$, the average standard deviation of the current was 0.002879 nA for Figure 3A at a bias region of ± 1.0 V. A plot of the current calculated with the Simmons equation was obtained under 95% confidence. Plots comparing the average current obtained at $0.0 < V < +1.0$ for junctions with STM (Figure S5 in the Supporting Information, respective to Figure 3A,D) to the current calculated with the Simmons equation imply good agreement of the experimental data with the model. A nonlinear regression of the current fitting was carried out, yielding values in excess of 98% (*i.e.*, *R*-square values of >0.98) for the fitting parameters (Table S2A, Supporting Information). Therefore, for $\alpha \neq 1$, the modified rectangular model was well fitted to the experimental data.

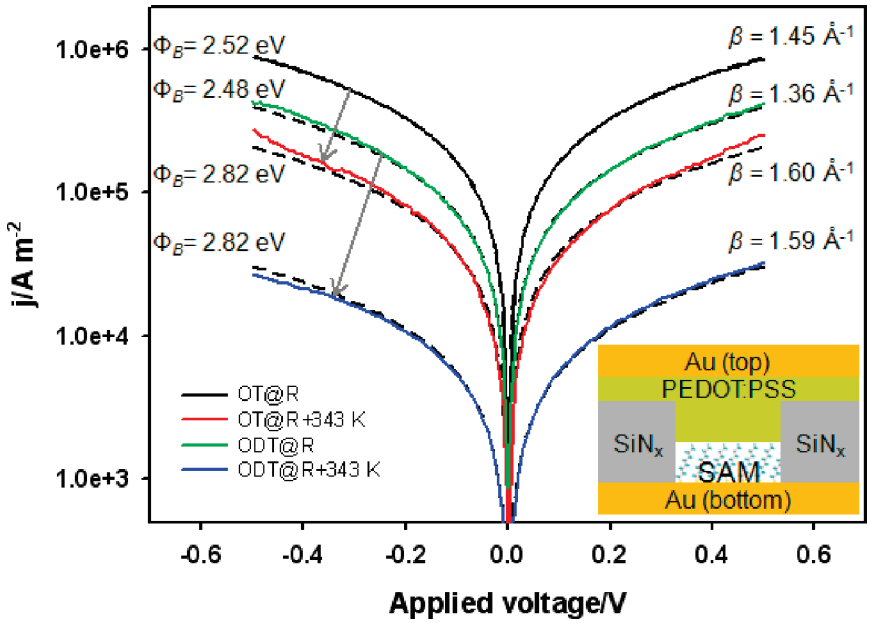

Figure 4. *J*−*V* characteristics obtained through micropore junctions (an active area of 0.49 nm^2 with a 25 μm diameter) of OT and ODT SAMs prepared in a 1 mM solution at room temperature for 2 h (OT@R and ODT@R) and additionally immersed at 343 K for 2 h (OT@R+343 K and ODT@R+343 K). Current density is plotted against the applied voltage on a log scale. The dotted lines represent the fits obtained using the Simmons model. *J*−*V* curves are the average of 20 curves for each SAM. The inset is a side-view of a micropore-based molecular junction of an alkanethiol SAM using a PEDOT:PSS film.

For the hexagonal closed phase (*i.e.*, c(4$\sqrt{3}$ × 2$\sqrt{3}$) at room temperature) on OT SAMs, the parameters of the Simmons model ($\alpha \neq 1$) that fit the $I-V$ curves at a low bias of ± 1.0 V were found to be $\Phi_B \approx 1.49$ eV and $\alpha \approx 0.80$, and the β value at zero voltage was estimated to be 1.00 Å^{-1} (Figure 3A). Furthermore, $\Phi_B \approx 1.69$ eV, $\alpha \approx 0.76$, and $\beta \approx 1.02$ Å^{-1} were obtained by the $I-V$ curves fitted at a low bias of ± 1.0 V for the striped phase (*i.e.*, (6 × $\sqrt{3}$) at 343 K) on OT SAMs (Figure 3C). The tunneling barrier in individual OT molecular junctions increased in the striped phase after the phase transition from the hexagonal closed phase. However, a combination of Φ_B and α yielded a similar β value. The β values calculated using the Simmons models for single OT junctions are comparable with results of an earlier report concerning alkanethiols obtained with STM ($\beta = 1.20$ Å^{-1}).[26] Thus, we believe that the goal of this work to compare the differences in $I-V$ behavior (*e.g.*, the tunneling barrier and the tunneling decay constant) between the two structural phases can be accomplished by application of the Simmons model.

For the c(4$\sqrt{3}$ × 2$\sqrt{3}$) and (6 × $\sqrt{3}$) phases on ODT SAMs (Figure 3B,D), the Simmons fit $I-V$ curves ($\alpha \neq 1$) reveal similar electronic characteristics at a low bias region of ± 1.0 V. $\Phi_B \approx 1.39$ eV, $\alpha \approx 0.73$, and $\beta \approx 0.89$ Å^{-1} for ODT in the hexagonal closed c(4$\sqrt{3}$ × 2$\sqrt{3}$) phase and $\Phi_B \approx 1.42$ eV, $\alpha \approx 0.74$, and $\beta \approx 0.90$ Å^{-1} for ODT in the striped (6 × $\sqrt{3}$) phase were estimated by Simmons fitting to the measured $I-V$ curves. The tunneling barrier in individual ODT molecular junctions is not strongly influenced by the phase transition.

On the basis of the results from the STM-based junction, it is determined that electronic characteristics of thiolate molecules contribute to intermolecular coupling in monolayer phases. Thus, it is expected that the multiple intermolecular coupling in thiolate SAMs for a large area junction will significantly influence electronic transport.

To examine molecular electron tunneling through a large junction area according to a change of monolayer phases, a micropore-based large molecular junction was fabricated, as depicted in the inset of Figure 4 (a vertical structure of Au/PEDOT:PSS/SAM/Au in a micropore insulated with a silicon nitride layer, see Figure S6, Supporting Information).[27,28] For fabrication of micropore junctions with different phases of thiolate SAMs, a conducting polymer, PEDOT:PSS (poly(3,4-ethylenedioxythiophene):poly(4-styrenesulfonic

acid), was used as a junction contact at the top electrode, preventing the formation of a short circuit between the bottom and top contacts. The PEDOT:PSS film has a contact resistance, which results in an increase of the contact barrier. However, $I-V$ characteristics for only PEDOT:PSS films show ohmic conduction, and the thiolate-inserted molecular M−I−M junctions with the PEDOT:PSS film show reproducibly discriminated $I-V$ characteristics corresponding to each thiolate SAM.

The Simmons model was fitted to current density plots *versus* applied voltage ($J-V$) (Figure 4). The Simmons fit curves show that the modified rectangular barrier model fits the $J-V$ curves at a low bias region of ± 0.5 V. Molecular electronic characteristics through each monolayer phase are compared with the fitting parameters (Φ_B and α) and the estimated β values. The estimated tunneling parameters (Table S2B, Supporting Information) indicate that both the OT and ODT molecular junctions have a larger tunneling barrier and a higher tunneling decay constant in the striped phases than in the hexagonal closed phases. These results reveal monolayer phase-dependent tunneling characteristics in a large junction. For the hexagonal closed phase on OT SAMs (formed at room temperature), the extracted parameters of the Simmons model fit to the $J-V$ curves were found to be $\Phi_B \approx 2.52$ eV and the β value at zero voltage was estimated to be 1.45 $Å^{-1}$ (the black curve in Figure 4). For the striped phase on OT SAMs (formed at room temperature +343 K), $\Phi_B \approx 2.82$ eV and $\beta \approx 1.60$ $Å^{-1}$ were obtained by the fitted $J-V$ curves (the red curve in Figure 4). Furthermore, in the case of ODT SAMs, $\Phi_B \approx 2.48$ eV and $\beta \approx 1.36$ $Å^{-1}$ were obtained in the hexagonal closed phase, and $\Phi_B \approx 2.82$ eV and $\beta \approx 1.59$ $Å^{-1}$ were obtained in the striped phase.

The tunneling pathway through an alkanethiol SAM can be explained in terms of through-bond tunneling and through-space (or chain-to-chain) tunneling.[2,12,14] If thiolate molecules in a SAM are individually isolated so as to negate the influence of surrounding molecules, the isolated single molecules should have the same tunneling distance and the tunneling pathway will be dominated by through-bond tunneling. The missing molecular lines in the striped phase lead to an increase in the tilting angle. The molecules in the striped ($6 \times \sqrt{3}$) phase are expected to be oriented at a tilt angle larger than ~30° with respect to the surface normal in the hexagonal closed c($4\sqrt{3} \times 2\sqrt{3}$) phase. A change in the tunneling pathway through the molecular junctions may be induced by a tilt of the chains. This may lead to a change in the tunneling distance through the molecular junctions, which will affect the tunneling barrier at the contacts. An increase in the molecular tilt angle in the striped ($6 \times \sqrt{3}$) phase for OT SAMs will induce a decrease in the monolayer thickness, resulting in an increase in the tunneling distance *via* the through-space tunneling (*i.e.*, intermolecular coupling).[2] As the tunneling distance becomes longer, the junction conductance becomes smaller. Thus, the similar β values of the two phases in the OT and ODT individual molecular junctions indicate that there are no significant changes in the tunneling distance.

A tilt of the chains can also affect the junction resistance, resulting in a change of the potential barrier at the contacts. According to findings reported in the literature, the junction contact can affect molecules in molecular junctions, which results in a change in the β value.[2,12] For example, in an alkanedithiol molecular junction in which the dominant transport pathway will be through-bond tunneling in an alkanedithiol SAM, the effects of the chemical contact played an important role, resulting in an increase in the junction conductance compared to an instance of physical contact.[12] Therefore, the terminal thiol (SH) group of ODT can play a critical role in the tunneling, possibly resulting in larger electronic coupling relative to the terminal methyl (CH_3) group of OT at the junction contact with the STM tip. The tunneling decay constant β of the ODT molecular junctions is expected to be lower than that of the OT molecular junctions.

Molecule tilting can induce intermolecular coupling, resulting in a decrease of the through-bond tunneling portion in the tunneling pathway. Considering a change in the monolayer thickness caused by tilting molecules, through-space tunneling becomes important in junction conductance. The tunneling distance in through-space tunneling, in which electrons pass across the monolayer by means of intermolecular transfer to neighboring chains lying in the shortest path for tunneling, is longer than that in through-bond tunneling, in which the electrons pass along the backbone of the alkane chains. The tunneling decay constant β value is associated with a change in the tunneling distance combined with the through-bond tunneling and the through-space tunneling. The β value for through-space tunneling was found to be higher than that for through-bond tunneling.[2,12,14] For example, Slowinski *et al.*[14] reported that the β value of through-bond was 0.91 $Å^{-1}$, whereas that of a through-space was 1.31 $Å^{-1}$. Therefore, it is believed that through-space tunneling is important in monolayer-based junctions. The monolayer-based tunneling characteristics in the micropore junction revealed multiple intermolecular coupling effects on the tunneling distance. In contrast to the case of the STM-based molecular individual junctions, an increase in the intermolecular coupling due to the phase transition clearly influences the tunneling pathway in the large molecular junctions. Consequently, the values of tunneling characteristics for the OT and ODT SAMs indicate that the phase transition from c($4\sqrt{3} \times 2\sqrt{3}$) (or ($\sqrt{3} \times \sqrt{3}$)) to ($6 \times \sqrt{3}$) leads to a relative decrease in the through-bond tunneling (even monolayer

thickness decreases) while the intermolecular coupling increases.

In addition, the current density value through the hexagonal closed phase on the ODT SAMs is lower than that through the same phase on the OT SAMs. The decrease in the current density of the ODT molecular junction is larger than that of the OT molecular junction, indicating that electron transport through ODT SAMs is more sensitive to structural phase transition than that through OT SAMs. This is shown in the STM images (Figure S2, Supporting Information) of ODT SAMs compared to OT SAMs. Similar to the effect of defects in a SAM, numerous small domain boundaries (in the hexagonal closed phase) and kinks in molecular rows (in the striped phase) will lead to a decrease of the current density through a large molecular junction of ODT SAMs relative to OT SAMs. Therefore, it is believed that in a large molecular junction, the structural phase transition induces a decrease of the current density through the molecular junction by physical defects of the SAMs and an increase of the contact barrier by the integrated intermolecular coupling.

In summary, the structural phase transition from a hexagonal closed phase to a striped phase in thiolate SAMs on gold was characterized by STM imaging and water contact angle measurements. Variation in electron tunneling characteristics according to the structural phase was measured in STM-based individual molecular junctions and micropore-based large molecular junctions. The effect of multiple intermolecular coupling on the electronic characteristics of thiolate molecules in a large area junction clearly appeared with monolayer phases. The phase transition induces an increase in the tunneling barrier height and the tunneling decay constant, which indicates an increase in intermolecular coupling between neighboring molecules in the striped phase or a decrease of monolayer thickness. Our results provide insight into the effect of intermolecular coupling on tunneling characteristics according to a change of monolayer phases for monolayer-based molecular electronic applications.

EXPERIMENTAL METHODS

Preparation of Self-Assembled Monolayers on Gold Substrates. Au(111)/mica substrates (Molecular Imaging) were used for scanning tunneling microscopy (STM) measurements. Au(800 Å)/Si(100) substrates were used for contact angle measurements (Surface Electro Optics, Phoenix-300). The gold substrates were cleaned with a hot piranha solution (1:3 H_2O_2 (Junsei) and H_2SO_4 (Junsei)) (Caution: piranha solution is a very strong oxidant, is extremely dangerous, and should be handled with great care), washed with deionized (DI) water (18.2 MΩ · cm, Millipore) and ethanol (J. T. Baker), and dried with a N_2 stream. The cleaned Au(111)/mica substrates were annealed by a propane flame prior to use. All SAMs were formed in 1 mM solutions of 1-octanethiol (Aldrich) and 1,8-octanedithiol (Aldrich), washed with ethanol and DI water thoroughly, and dried with a N_2 stream. SAMs on the Au/Si substrates before and after heat treatment were characterized by X-ray photoelectron spectroscopy (Figure S7, Supporting Information).

Fabrication of Micropore-Based Molecular Junction Devices. (1) Micropores of 25 μm in diameter with a gold bottom electrode (insulated by a SiNx layer) were fabricated as described in a previous report.[29] (2) Molecular junctions through SAMs on the gold bottom electrode of the micropores were prepared *via* the following process: micropores were cleaned by ultrasonication (Branson) in acetone (J. T. Baker) at 313 K for 20 min, chemically cleaned with a hot piranha solution, washed with DI water and ethanol, and then dried with a N_2 stream. The preparation of SAMs on micropores was carried out as described above. All SAMs on micropores were dried under a vacuum for 2 h at least. The molecular junctions through the SAMs on micropores were produced with a spin-coated PEDOT:PSS ((poly(3,4-ethylenedioxythiophene):poly(4-styrenesulfonic acid), Baytron P HC V4, H.C. Starck GmbH & Co.) film and an evaporated gold top electrode (>80 nm thick) (Figure S6, Supporting Information). The PEDOT:PSS solution was prepared with 5−10% DMSO (J. T. Baker) and 0.1−0.2% nonionic surfactant (FSO Zonyl 100, Dupont) to improve the conductivity and the wettability of the film to the SAMs. The PEDOT:PSS solution was sonicated for at least 20 min and then filtered with a syringe filter. The spin-coated PEDOT:PSS film was dried under a vacuum overnight before evaporation deposition of a gold top electrode.

***I*−*V* Measurements.** Electrochemical etched Pt/Ir tips (Molecular Imaging) were used for scanning tunneling microscopy (STM) measurements (Omicron, VT STM). STM was performed at room temperature under an ultrahigh vacuum ($<1.5 \times 10^{-10}$ torr). *I*−*V* measurements for micropores were performed using a Keithley 4200 analyzer at room temperature.

Acknowledgment. This work was supported by the Creative Research Initiatives (project title: Smart Molecular Memory) of MEST (Ministry of Education Science and Technology)/KOSEF (Korea Science and Engineering Foundation). The authors acknowledge H. Chang and S. Kim for fabrication of micropores.

Supporting Information Available: STM images (Figures S1 and S2), *I*−*V* curves taken from a single molecular junction at various tunneling currents (Figure S3), *I*−*V* curves on a log scale for individual molecular junctions (Figure S4), *R*-squared values of fitting curves (Figure S5), cross-sectional views of micropore-based junctions (Figure S6), XPS data (Figure S7), water contact angle data (Table S1), and tunneling parameters obtained from the Simmons model fitting (Table S2). This material is available free of charge *via* the Internet at http://pubs.acs.org.

REFERENCES AND NOTES

1. Cui, X. D.; Primak, A.; Zarate, X.; Tomfohr, J.; Sankey, O. F.; Moore, A. L.; Moore, T. A.; Gust, D.; Harris, G.; Lindsay, S. M. Reproducible Measurement of Single-Molecule Conductivity. *Science* **2001**, *294*, 571–574.
2. Salomon, A.; Cahen, D.; Lindsay, S.; Tomfohr, J.; Engelkes, V. B.; Frisbie, C. D. Comparison of Electronic Transport Measurements on Organic Molecules. *Adv. Mater.* **2003**, *15*, 1881–1890.
3. Engelkes, V. B.; Beebe, J. M.; Frisbie, C. D. Length-Dependent Transport in Molecular Junctions Based on SAMs of Alkanethiols and Alkanedithiols: Effect of Metal Work Function and Applied Bias on Tunneling Efficiency and Contact Resistance. *J. Am. Chem. Soc.* **2004**, *126*, 14287–14296.
4. Galperin, M.; Ratner, M. A.; Nitzan, A.; Troisi, A. Nuclear Coupling and Polarization in Molecular Transport Junctions: Beyond Tunneling to Function. *Science* **2008**, *319*, 1056–1060.
5. Song, H.; Lee, H.; Lee, T. Intermolecular Chain-to-Chain Tunneling in Metal−Alkanethiol−Metal Junctions. *J. Am. Chem. Soc.* **2007**, *129*, 3806–3807.

6. Wang, W.; Lee, T.; Reed, M. A. Mechanism of Electron Conduction in Self-Assembled Alkanethiol Monolayer Devices. *Phys. Rev. B* **2003**, *68*, 354161–354167.
7. Wang, W.; Lee, T.; Reed, M. A. Elastic and Inelastic Electron Tunneling in Alkane Self-Assembled Monolayers. *J. Phys. Chem. B* **2004**, *108*, 18398–18407.
8. Jeremy, M. B.; BongSoo, K.; Gadzuk, J. W.; Frisbie, C. D.; James, G. K. Transition from Direct Tunneling to Field Emission in Metal−Molecule−Metal Junctions. *Phys. Rev. Lett.* **2006**, *97*, 026801.
9. Holmlin, R. E.; Haag, R.; Chabinyc, M. L.; Ismagilov, R. F.; Cohen, A. E.; Terfort, A.; Rampi, M. A.; Whitesides, G. M. Electron Transport through Thin Organic Films in Metal−Insulator−Metal Junctions Based on Self-Assembled Monolayers. *J. Am. Chem. Soc.* **2001**, *123*, 5075–5085.
10. Selzer, Y.; Cai, L.; Cabassi, M. A.; Yao, Y.; Tour, J. M.; Mayer, T. S.; Allara, D. L. Effect of Local Environment on Molecular Conduction: Isolated Molecule *versus* Self-Assembled Monolayer. *Nano Lett.* **2005**, *5*, 61–65.
11. Beebe, J. M.; Kim, B.; Frisbie, C. D.; Kushmerick, J. G. Measuring Relative Barrier Heights in Molecular Electronic Junctions with Transition Voltage Spectroscopy. *ACS Nano* **2008**, *2*, 827–832.
12. Cui, X. D.; Zarate, X.; Tomfohr, J.; Sankey, O. F.; Primak, A.; Moore, A. L.; Moore, T. A.; Gust, D.; Harris, G.; Lindsay, S. M. Making Electrical Contacts to Molecular Monolayers. *Nanotechnology* **2002**, *13*, 5–14.
13. Lindstrom, C. D.; Muntwiler, M.; Zhu, X. Y. Electron Transport Across the Alkanethiol Self-Assembled Monolayer/Au(111) Interface: Role of the Chemical Anchor. *J. Phys. Chem. B* **2005**, *109*, 21492–21495.
14. Slowinski, K.; Chamberlain, R. V.; Miller, C. J.; Majda, M. Through-Bond and Chain-to-Chain Coupling. Two Pathways in Electron Tunneling through Liquid Alkanethiol Monolayers on Mercury Electrodes. *J. Am. Chem. Soc.* **1997**, *119*, 11910–11919.
15. Poirier, G. E. Coverage-Dependent Phases and Phase Stability of Decanethiol on Au(111). *Langmuir* **1999**, *15*, 1167–1175.
16. Poirier, G. E.; Fitts, W. P.; White, J. M. Two-Dimensional Phase Diagram of Decanethiol on Au(111). *Langmuir* **2001**, *17*, 1176–1183.
17. Qian, Y.; Yang, G.; Yu, J.; Jung, T. A.; Liu, G. y. Structures of Annealed Decanethiol Self-Assembled Monolayers on Au(111): An Ultrahigh Vacuum Scanning Tunneling Microscopy Study. *Langmuir* **2003**, *19*, 6056–6065.
18. Yang, G.; Liu, G. y. New Insights for Self-Assembled Monolayers of Organothiols on Au(111) Revealed by Scanning Tunneling Microscopy. *J. Phys. Chem. B* **2003**, *107*, 8746–8759.
19. Nicholas, C., III; Christopher, E. D. C.; Gang-yu, L.; Giacinto, S. Superlattice Structure at the Surface of a Monolayer of Octadecanethiol Self-Assembled on Au(111). *J. Chem. Phys.* **1993**, *98*, 3503–3511.
20. Poirier, G. E.; Tarlov, M. J. The c(4 × 2) Superlattice of *n*-Alkanethiol Monolayers Self-Assembled on Au(111). *Langmuir* **1994**, *10*, 2853–2856.
21. McCreery, R. L. Molecular Electronic Junctions. *Chem. Mater.* **2004**, *16*, 4477–4496.
22. Simmons, J. G. Generalized Formula for the Electric Tunnel Effect between Similar Electrodes Separated by a Thin Insulating Film. *J. Appl. Phys.* **1963**, *34*, 1793–1803.
23. Lee, T.; Wang, W.; Reed, M. A. Mechanism of Electron Conduction in Self-Assembled Alkanethiol Monolayer Devices. *Ann. N.Y. Acad. Sci.* **2003**, *1006*, 21–35.
24. Dameron, A. A.; Ciszek, J. W.; Tour, J. M.; Weiss, P. S. Effects of Hindered Internal Rotation on Packing and Conductance of Self-Assembled Monolayers. *J. Phys. Chem. B* **2004**, *108*, 16761–16767.
25. Akkerman, H. B.; Naber, R. C. G.; Jongbloed, B.; van Hal, P. A.; Blom, P. W. M.; de Leeuw, D. M.; de Boer, B. Electron Tunneling through Alkanedithiol Self-Assembled Monolayers in Large-Area Molecular Junctions. *Proc. Natl. Acad. Sci. U.S.A.* **2007**, *104*, 11161–11166.
26. Bumm, L. A.; Arnold, J. J.; Dunbar, T. D.; Allara, D. L.; Weiss, P. S. Electron Transfer through Organic Molecules. *J. Phys. Chem. B* **1999**, *103*, 8122–8127.
27. Akkerman, H. B.; Blom, P. W. M.; de Leeuw, D. M.; de Boer, B. Towards Molecular Electronics with Large-Area Molecular Junctions. *Nature* **2006**, *441*, 69–72.
28. Akkerman, H. B.; Kronemeijer, A. J.; van Hal, P. A.; de Leeuw, D. M.; Blom, P. W. M.; de Boer, B. Self-Assembled-Monolayer Formation of Long Alkanedithiols in Molecular Junctions. *Small* **2008**, *4*, 100–104.
29. Kim, D. H.; Lee, H.; Song, C. K.; Lee, C. Fabrication of Nanosized Molecular Array Device and Logic Gate Using Dimethyl-phenylethynyl Thiol. *J. Nanosci. Nanotechnol.* **2006**, *6*, 3470–3474.